THE LARGE DEFLECTION OF A RIGID–PERFECTLY PLASTIC PORTAL FRAME SUBJECTED TO IMPULSIVE LOADING

Q. ZHOU, T. X. YU and HUANG ZHUPING

Department of Mechanics, Peking University, Beijing 100871, P.R. China

Abstract—A portal frame subjected to a distributed impulse is studied on the basis of a large deflection formulation. By assuming that the material is rigid–perfectly plastic, a complete solution is constructed and then compared with the modal solution and the experimental results reported by Hashmi and Al-Hassani (1975, *Int. J. Mech. Sci.* **17**, 513–523) and Bodner and Symonds (1979, *Int. J. Solids Structures* **15**, 1–13). The solution agrees well with the experimental results and indicates that a great part of the input energy is absorbed by travelling plastic hinges. The possible failure regions are discussed according to the distribution of plastic work.

NOTATION

b	width
E	Young's modulus
E_0	initial kinetic energy $mL_1 V_0^2$
E_k^*	kinetic energy in second phase
E_k	non-dimensional kinetic energy in second phase E_k^*/E_0
E_{k1}^*	kinetic energy at the end of the first phase
E_{k1}	non-dimensional kinetic energy at the end of the first phase E_{k1}^*/E_0
H	thickness
I	impulse of loading
I_1^*, I_2^*	static moments of segment GB with respect to W_1- and U_1-axis, respectively
I_1, I_2	non-dimensional quantities I_1^*/mL_1^2 and I_2^*/mL_1^2, respectively
I_G^*	moment of inertia of segment GB with respect to G
I_G	non-dimensional quantity I_G^*/mL_1^3
J	moment of inertia of the cross-section of the beam
J_1^*, J_2^*	static moments of segment HB with respect to W_2- and U_2-axis, respectively
J_1, J_2	non-dimensional quantities J_1^*/mL_2^2 and J_2^*/mL_2^2, respectively
J_H^*	moment of inertia of segment HB with respect to H
J_H	non-dimensional quantity J_H^*/mL_2^3
L_1	half-span length of the frame
L_2	height of the frame
M_0	dynamic fully plastic bending moment of the beam
m	mass of beam per unit length
N_1, N_2	axial forces in horizontal and vertical beam, respectively
R	$E_0/$(maximum elastic strain energy the structure can store)
T_0	$mL_1^2 V_0/M_0$
t	time
t_1	the time taken by the first phase
V_0	initial velocity
V^*	the velocity of midpoint C in the second phase
V	non-dimensional velocity V^*/V_0
U_1, W_1	local coordinates of deformed horizontal beam
U_1', W_1'	local coordinates of deformed horizontal beam at the end of the first phase
U_2, W_2	local coordinates of deformed vertical beam
x_1, x_2	arc lengths of PB and QB, respectively
y_1, y_2	arc lengths of GB and HB, respectively
y_{21}	arc length of deformed vertical beam at the end of the first phase
α	non-dimensional initial kinetic energy E_0/M_0
β	angle defined in Fig. 4
β_f	final value of β
γ	the ratio L_2/L_1
$\dot{\varepsilon}$	strain rate
η_1, η_2	non-dimensional quantities y_1/L_1 and y_2/L_2
η_{21}	non-dimensional quantity y_{21}/L_2
θ_1, θ_2	angles defined in Fig. 2
θ_{10}	the angle between the tangent of arc GB at B and the U_1-axis

θ_{20} the angle between the tangent of arc HB at B and the L'_2-axis
κ_1^*, κ_2^* curvature changes of GB and HB, respectively
κ_1, κ_2 non-dimensional curvature changes $\kappa_1^* L_1$ and $\kappa_2^* L_2$
ρ density of material
σ dynamic yield stress of material
σ_0 yield stress of material
τ non-dimensional time t/T_0
τ_1 non-dimensional time taken by the first phase t_1/T_0
ω angular velocity.

INTRODUCTION

The plastic behavior of portal frames under dynamic loading is of importance in many engineering problems, and so has been studied extensively by various methods. A classical example is the study of the large plastic deflection response of portal frames to distributed impulsive loading (see Fig. 1). Hashmi and Al-Hassani (1975) studied this problem experimentally. Their frame specimens were made of aluminium while the loading was exerted by magnetomotive impulse. Bodner and Symonds (1979) also carried out experiments on portal frames by means of explosive loading. Their frame specimens were made of mild steel and titanium, both having rate-sensitive plastic behavior.

On the theoretical side of this problem, Symonds and Chon (1979) proposed a modal solution on the basis of large viscoplastic deflections. The results of their theory agree well with the experimental results reported by Bodner and Symonds (1979). At the same time, Symonds and Raphanel (1979) studied this problem using the simplified elastic–plastic method (SEP). The second phase of the SEP solution corresponds to the modal solution of large deflection, while the material is assumed to be rigid–perfectly plastic in this phase.

In the literature, there is no complete solution which satisfies all the field equations of dynamics, compatibility, end conditions at supports, plastic behavior of materials and initial conditions of this problem. Obviously, to obtain the complete solution, some idealizations are necessary. When the energy dissipated in plastic work in a frame greatly exceeds the elastic strain energy the frame can store, it is reasonable to neglect the elastic deformation and to start with the assumption that the material of the frame is rigid–plastic.

The earliest analysis adopting the rigid–plastic idealization and the concept of the travelling plastic hinge was by Lee and Symonds (1952), who considered a free–free uniform beam subjected to a transverse pulse applied at its midpoint. The concept of the travelling plastic hinge has been widely used in structural dynamic problems, e.g. the study by Symonds and Mentel (1958) of the response of rigid–perfectly plastic beams under a distributed impulsive loading.

Under intense dynamic loading, the structure usually undergoes large deflections, so the theoretical predictions may agree with the experimental results only when the geometrical effects due to large deflections are taken into account. Ting (1965) made the first attempt to construct a complete solution to a rigid–perfectly plastic cantilever impinged by a rigid mass at its tip on the basis of a large deflection formulation. Yu *et al.* (1985, 1986) examined the dynamic response of a quadrantal circular beam subjected to a radial impact in its own plane at its tip by a rigid mass, and Zhang and Yu (1986) investigated the large
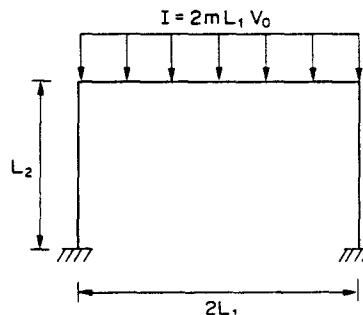

Fig. 1. A portal frame subjected to impulsive loading on its horizontal beam.

deflection solution of the same problem. These investigations indicate that the geometrical changes in the structures may reduce the final deflection significantly.

Many non-linear finite element programs have been developed recently. Although they can compute the dynamic plastic response of structures including the effects of elasticity, strain hardening, strain rate and geometrical non-linearity, they are time consuming when an impulsive problem, especially involving an initial velocity discontinuity, is computed. If the rigid–plastic complete solution of a dynamic problem can be given and compared with its finite element solution and/or the experimental results, it is certainly helpful in understanding the underlying mechanisms of the problem.

The aim of the present study is to analyse the dynamic response of a rigid–perfectly plastic portal frame subjected to a distributed impulsive loading (Fig. 1) on the basis of a large deflection formulation. The complete solution is constructed and compared with the results of the modal solution presented by Symonds and Raphanel (1979) and the experimental results reported by Hashmi and Al-Hassani (1975) and Bodner and Symonds (1979). Adopting only the large deflection formulation, the theoretical results will be closer to the true circumstances and the vertical beam will deform (see the Discussions section). The final shape of the complete solution is closer to the experimental results than the modal solution and the regions where failure may occur can be found according to the distribution of plastic work.

ASSUMPTIONS

Suppose the frame has uniform cross-section and assume that:

(i) the frame is rigid–perfectly plastic;
(ii) the material is rate-independent, so that the dynamic fully plastic bending moment M_0 is a constant for all strain rates;
(iii) the influence of shear and axial forces on yielding can be neglected;
(iv) the strain is very small, so that the relationship between the strain and the derivative of the displacement is linear;
(v) the deflection is large, so that the dynamic equations and geometrical relations are established according to the deformed configuration.

The impulsive loading shown in Fig. 1 is equivalent to giving a distributed initial velocity V_0 to the horizontal beam of the frame.

Due to the symmetry of the problem, only one half of the frame is analysed in the following.

The initial kinetic energy of the frame is supposed to be dissipated by plastic bending and this, therefore, implies a plastic hinge or hinges.

Assume the deformation model is as shown in Fig. 2. Initially, two plastic hinges start
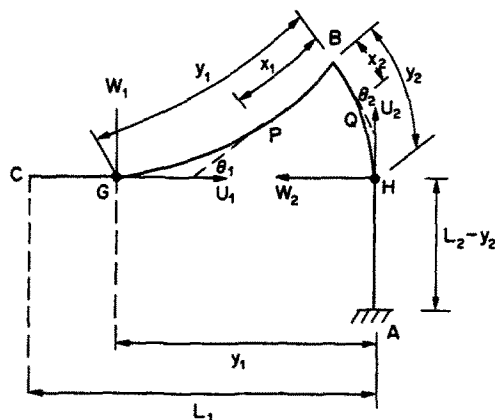

Fig. 2. The geometrical configuration of a half-portal frame after its large deflection in the first phase. Points G and H denote the positions of the travelling plastic hinges at time t.

to travel simultaneously from corner B. One moves along the horizontal beam towards midpoint C, and reaches position G at time t. The other moves along the vertical beam towards base A, and reaches position H at time t. Segment CG moves transversely downwards as a rigid body. The following analysis confirms that it moves with initial velocity V_0. Segment GBH rotates about H at time t. Since the velocity at point G should be along the vertical direction, point H must be at the same height as that of point G. It is quite evident that neither of the travelling plastic hinges stops initially at corner B for the compatibility of deformation on the basis of a large deflection to hold, and that the angle between arc GB and arc HB retains rectangular because there is no rotation angle discontinuity after the travelling plastic hinges pass by. When hinge G reaches midpoint C, the first phase ends and the second phase starts. The deformation model in the second phase has a fixed plastic hinge at midpoint C, and hinge H continues to move as it did in the first phase. H is still at the same height as that of point C. The second phase ends when all the kinetic energy is dissipated. Here we suppose that the vertical beam BA is so long that the travelling hinge H will not reach base A by the end of the response. The experiments reported by Hashmi and Al-Hassani (1975) and Bodner and Symonds (1979) and the following computing examples indicate that the plastic deformation will usually not propagate to base A within the interested range of the ratio $\gamma = L_2/L_1$ in most engineering circumstances.

FORMULATION

First phase

As shown in Fig. 2, we establish the coordinate systems U_1GW_1 and U_2HW_2, which move transversely with travelling hinges G and H, respectively. The unit vectors in the systems satisfy

$$\begin{cases} \mathbf{i}_1 = -\mathbf{j}_2 \\ \mathbf{j}_1 = \mathbf{i}_2 \\ \mathbf{k}_1 = \mathbf{k}_2. \end{cases} \tag{1}$$

P and Q are arbitrary points in the arcs GB and HB, respectively. According to Fig. 2 and the Notation section, we have

$$\begin{cases} \theta_1(x_1, y_1) = \int_{x_1}^{y_1} \kappa_1^*(x_1) \, dx_1 \\ \theta_2(x_2, y_2) = \int_{x_2}^{y_2} \kappa_2^*(x_2) \, dx_2 \end{cases} \tag{2}$$

$$\begin{cases} U_1(x_1, y_1) = \int_{x_1}^{y_1} \cos \theta_1(x_1, y_1) \, dx_1 \\ W_1(x_1, y_1) = \int_{x_1}^{y_1} \sin \theta_1(x_1, y_1) \, dx_1 \end{cases} \tag{3}$$

$$\begin{cases} U_2(x_2, y_2) = \int_{x_2}^{y_2} \cos \theta_2(x_2, y_2) \, dx_2 \\ W_2(x_2, y_2) = \int_{x_2}^{y_2} \sin \theta_2(x_2, y_2) \, dx_2 \end{cases} \tag{4}$$

$$\begin{cases} I_1^*(y_1) = \int_0^{y_1} m U_1(x_1, y_1) \, dx_1 \\[2mm] I_2^*(y_1) = \int_0^{y_1} m W_1(x_1, y_1) \, dx_1 \\[2mm] I_G^*(y_1) = \int_0^{y_1} m[U_1^2(x_1, y_1) + W_1^2(x_1, y_1)] \, dx_1 \end{cases} \tag{5}$$

$$\begin{cases} J_1^*(y_2) = \int_0^{y_2} m U_2(x_2, y_2) \, dx_2 \\[2mm] J_2^*(y_2) = \int_0^{y_2} m W_2(x_2, y_2) \, dx_2 \\[2mm] J_H^*(y_2) = \int_0^{y_2} m[U_2^2(x_2, y_2) + W_2^2(x_2, y_2)] \, dx_2. \end{cases} \tag{6}$$

It follows that

$$\begin{cases} \dfrac{\partial U_1(x_1, y_1)}{\partial y_1} = 1 - \kappa_1^*(y_1) W_1(x_1, y_1) \\[3mm] \dfrac{\partial W_1(x_1, y_1)}{\partial y_1} = \kappa_1^*(y_1) U_1(x_1, y_1) \end{cases} \tag{7}$$

$$\begin{cases} \dfrac{dI_1^*(y_1)}{dy_1} = m y_1 - \kappa_1^*(y_1) I_2^*(y_1) \\[3mm] \dfrac{dI_2^*(y_1)}{dy_1} = \kappa_1^*(y_1) I_1^*(y_1) \\[3mm] \dfrac{dI_G^*(y_1)}{dy_1} = 2 I_1^*(y_1) \end{cases} \tag{8}$$

$$\begin{cases} \dfrac{\partial U_2(x_2, y_2)}{\partial y_2} = 1 - \kappa_2^*(y_2) W_2(x_2, y_2) \\[3mm] \dfrac{\partial W_2(x_2, y_2)}{\partial y_2} = \kappa_2^*(y_2) U_2(x_2, y_2) \end{cases} \tag{9}$$

$$\begin{cases} \dfrac{dJ_1^*(y_2)}{dy_2} = m y_2 - \kappa_2^*(y_2) J_2^*(y_2) \\[3mm] \dfrac{dJ_2^*(y_2)}{dy_2} = \kappa_2^*(y_2) J_1^*(y_2) \\[3mm] \dfrac{dJ_H^*(y_2)}{dy_2} = 2 J_1^*(y_2). \end{cases} \tag{10}$$

Since the axial deformation is neglected, it is known that $\overline{GH} = y_1$ (see Fig. 2), so the transformation from $U_1 G W_1$ into $U_2 H W_2$ is given by

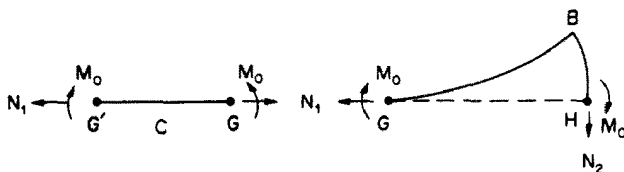$$\begin{cases} U_2 = W_1 \\ W_2 = y_1 - U_1. \end{cases} \tag{11}$$

Fig. 3. Forces acting on the portal frame.

Because the shear force at a travelling hinge is equal to zero, we have the force diagrams of segments CG and GBH as shown in Fig. 3.

Since there is no vertical force on segment CG, this segment must retain its initial velocity V_0; that is,

$$\mathbf{v_G} = -V_0\mathbf{j}_1 = -V_0\mathbf{i}_2. \tag{12}$$

Suppose $\omega = \omega\mathbf{k}_2$ is the angular velocity of the segment GBH at time t; thus we have

$$V_0 = \omega y_1. \tag{13}$$

Because H is always located at the same height as that of point G, we have

$$\dot{y}_2 = \frac{\mathrm{d}y_2}{\mathrm{d}t} = V_0. \tag{14}$$

Differentiating (2) with respect to t, we obtain

$$\begin{cases} \omega = \dot{\theta}_1 = \dot{y}_1\kappa_1^*(y_1) \\ \omega = \dot{\theta}_2 = \dot{y}_2\kappa_2^*(y_2) = V_0\kappa_2^*(y_2). \end{cases} \tag{15}$$

The velocity and acceleration of P and Q are

$$\mathbf{v_P} = \omega \times \mathbf{HP} = -\omega[y_1 - U_1(x_1,y_1)]\mathbf{i}_2 + \omega W_1(x_1,y_1)\mathbf{j}_2 \tag{16}$$

$$\dot{\mathbf{v}}_P = \{-\dot{\omega}[y_1 - U_1(x_1,y_1)] - \omega\dot{y}_1\kappa_1^*(y_1)W_1(x_1,y_1)\}\mathbf{i}_2$$
$$+ \{\dot{\omega}W_1(x_1,y_1) + \omega\dot{y}_1\kappa_1^*(y_1)U_1(x_1,y_1)\}\mathbf{j}_2 \tag{17}$$

and

$$\mathbf{v_Q} = \omega \times \mathbf{HQ} = -\omega W_2(x_2,y_2)\mathbf{i}_2 + \omega U_2(x_2,y_2)\mathbf{j}_2 \tag{18}$$

$$\dot{\mathbf{v}}_Q = \{-\dot{\omega}W_2(x_2,y_2) - \omega\dot{y}_2\kappa_2^*(y_2)U_2(x_2,y_2)\}\mathbf{i}_2 + [\dot{\omega}U_2(x_2,y_2)$$
$$+ \omega\dot{y}_2[1 - \kappa_2^*(y_2)W_2(x_2,y_2)]]\mathbf{j}_2, \tag{19}$$

respectively.

By applying D'Alembert's principle and referring to Fig. 3, conservation of momentum and the angular momentum give

$$\begin{cases} -N_2 - \int_0^{y_1} m\dot{\mathbf{v}}_P \cdot \mathbf{i}_2 \, \mathrm{d}x_1 - \int_0^{y_2} m\dot{\mathbf{v}}_Q \cdot \mathbf{i}_2 \, \mathrm{d}x_2 = 0 \\[2mm] N_1 - \int_0^{y_1} m\dot{\mathbf{v}}_P \cdot \mathbf{j}_2 \, \mathrm{d}x_1 - \int_0^{y_2} m\dot{\mathbf{v}}_Q \cdot \mathbf{j}_2 \, \mathrm{d}x_2 = 0 \\[2mm] -2M_0 - \mathbf{k}_2 \cdot \int_0^{y_1} \mathbf{HP} \times m\dot{\mathbf{v}}_P \, \mathrm{d}x_1 - \mathbf{k}_2 \cdot \int_0^{y_2} \mathbf{HQ} \times m\dot{\mathbf{v}}_Q \, \mathrm{d}x_2 = 0. \end{cases} \tag{20}$$

With the help of (5), (6), (17) and (19), (20) can be written as

$$\begin{cases} N_1 = I_2^*\dot{\omega}+\omega\dot{y}_1\kappa_1^*I_1^*+J_1^*\dot{\omega}+my_2\omega\dot{y}_2-\omega\dot{y}_2\kappa_2^*J_2^* \\ N_2 = my_1^2\dot{\omega}-I_1^*\dot{\omega}+\omega\dot{y}_1\kappa_1^*I_2^*+J_2^*\dot{\omega}+\omega\dot{y}_2\kappa_2^*J_1^* \\ 2M_0+I_G^*\dot{\omega}+my_1^3\dot{\omega}-2I_1^*y_1\dot{\omega}+\omega\dot{y}_1\dot{y}_1\kappa_1^*I_2^*+J_H^*\dot{\omega}+\omega\dot{y}_2J_1^* = 0. \end{cases} \tag{21}$$

Referring to (13), (14) and (15), we obtain

$$\kappa_1^* = \frac{V_0^2(I_G^*+J_H^*+my_1^3-2I_1^*y_1)}{y_1^2(2M_0y_1+J_1^*V_0^2+I_2^*V_0^2)} \tag{22}$$

$$\kappa_2^* = 1/y_1 \tag{23}$$

$$\dot{y}_1 = \frac{V_0}{y_1\kappa_1^*}. \tag{24}$$

The energy balance leads to

$$0.5m\left[L_1V_0^2-(L_1-y_1)V_0^2-\int_0^{y_1}\mathbf{v}_P\cdot\mathbf{v}_P\,dx_1-\int_0^{y_2}\mathbf{v}_Q\cdot\mathbf{v}_Q\,dx_2\right]$$
$$= M_0\int_0^{y_1}\kappa_1^*\,dx_1+M_0\int_0^{y_2}\kappa_2^*\,dx_2 \tag{25}$$

or, after tidying up,

$$V_0^2(2I_1^*y_1-I_G^*-J_H^*)/y_1^2 = 2M_0(\theta_{10}+\theta_{20}) \tag{26}$$

where

$$\begin{cases} \theta_{10} = \int_0^{y_1}\kappa_1^*\,dx_1 \\ \theta_{20} = \int_0^{y_2}\kappa_2^*\,dx_2. \end{cases} \tag{27}$$

It should be noted that $\theta_{10} = \theta_{20}$, because arc GB is perpendicular to arc HB at B. This implies that the plastic work dissipated in the horizontal beam is equal to that in the vertical beam at any instant, and so (26) results in

$$V_0^2(2I_1^*y_1-I_G^*-J_H^*)/y_1^2 = 4M_0\theta_{10}. \tag{28}$$

Indeed it can be proved that eqn (28) is equivalent to eqn (22).

In order to show the response of the frame in a general way, the non-dimensional quantities defined in the Notation section are used in non-dimensionalizing all the equations. For the sake of convenience in computation, the parameter η_1 is adopted as the

argument for the system of ordinary differential equations. Then we have

$$
\begin{cases}
\dfrac{d\tau}{d\eta_1} = \dfrac{\eta_1 \kappa_1}{\alpha} \\[2ex]
\dfrac{d\eta_2}{d\eta_1} = \dfrac{\eta_1 \kappa_1}{\gamma} \\[2ex]
\dfrac{dI_1}{d\eta_1} = \eta_1 - \kappa_1 I_2 \\[2ex]
\dfrac{dI_2}{d\eta_1} = \kappa_1 I_1 \\[2ex]
\dfrac{dI_G}{d\eta_1} = 2I_1 \\[2ex]
\dfrac{dJ_1}{d\eta_1} = \dfrac{\eta_1 \kappa_1}{\gamma}\left(\eta_2 - \dfrac{\gamma}{\eta_1}J_2\right) \\[2ex]
\dfrac{dJ_2}{d\eta_1} = J_1 \kappa_1 \\[2ex]
\dfrac{dJ_H}{d\eta_1} = \dfrac{2}{\gamma} J_1 \eta_1 \kappa_1
\end{cases}
\tag{29}
$$

where

$$
\kappa_1 = \frac{I_G + \gamma^3 J_H + \eta_1^3 - 2I_1\eta_1}{\eta_1^2(I_2 + \gamma^2 J_1 + 2\eta_1/\alpha)}.
\tag{30}
$$

The initial conditions for (29) are

$$
\eta_1 = 0, \quad \tau = \eta_2 = I_1 = I_2 = I_G = J_1 = J_2 = J_H = 0,
\tag{31}
$$

which form a singularity for eqns (29). To avoid this singularity, we start with η_1 being a small non-zero value to solve eqns (29). As proved in the Appendix, when η_1 is a small quantity, the values of the relevant quantities are

$$
\begin{cases}
\tau = \eta_1^2/6, \quad \eta_2 = \alpha\eta_1^2/6\gamma, \quad I_1 = \eta_1^2/2, \\
I_2 = \alpha\eta_1^3/36, \quad I_G = \eta_1^3/3, \quad J_1 = 0, \quad J_2 = 0, \quad J_H = 0.
\end{cases}
\tag{32}
$$

By taking $\eta_1 = 10^{-5}$, the initial values of the other quantities are specified by using (32). The system of first-order ordinary differential equations (29) can be integrated numerically by using a Runge–Kutta procedure until $\eta_1 = 1.0$, at which travelling plastic hinge G reaches midpoint C of the horizontal beam and the first phase ends.

Second phase

As shown in Fig. 4, the coordinate systems U_1CW_1 and U_2HW_2 are still in translational motion, while the coordinate system $U'_1CW'_1$ is fixed on arc CB, and the U'_1-axis is tangent to arc CB at C. The angle between the U_1-axis and the U'_1-axis is defined as β. It is evident that $\beta = 0$ when the second phase starts.

The transformation relation between the three coordinate systems is given by

$$
\begin{cases}
U_1 = U'_1 \cos\beta - W'_1 \sin\beta \\
W_1 = U'_1 \sin\beta + W'_1 \cos\beta
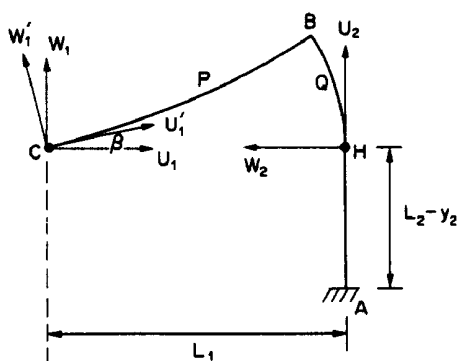\end{cases}
\tag{33}
$$

Fig. 4. The geometrical configuration of a half-portal frame after its large deflection in the second phase.

and

$$\begin{cases} U_2 = W_1 \\ W_2 = L_1 - U_1. \end{cases} \tag{34}$$

It is evident that

$$V^* = \omega L_1 \tag{35}$$

$$\dot{y}_2 = V^* \tag{36}$$

$$\omega = \dot{\beta} = \dot{y}_2 \kappa_2^* \tag{37}$$

where V^* is the velocity of midpoint C of the horizontal beam. Thus,

$$\kappa_2^* = 1/L_1 \tag{38}$$

$$\mathbf{v_P} = \omega \times \mathbf{HP}$$

$$= V^*/L_1 \{ -[L_1 - U_1'(x_1, L_1) \cos \beta + W_1'(x_1, L_1) \sin \beta] \mathbf{i}_2$$

$$+ [U_1'(x_1, L_1) \sin \beta + W_1'(x_1, L_1) \cos \beta] \mathbf{j}_2 \} \tag{39}$$

$$\mathbf{v_Q} = \omega \times \mathbf{HQ} = V^*/L_1 [-W_2(x_2, y_2)\mathbf{i}_2 + U_2(x_2, y_2)\mathbf{j}_2]. \tag{40}$$

Hence, the kinetic energy of segment CBH is

$$E_k^* = 0.5m \left(\int_0^{L_1} \mathbf{v_P} \cdot \mathbf{v_P} \, dx_1 + \int_0^{y_2} \mathbf{v_Q} \cdot \mathbf{v_Q} \, dx_2 \right)$$

$$= 0.5(V^*/L_1)^2 [I_C^*(L_1) + mL_1^3 - 2L_1 \cos \beta I_1^*(L_1) + 2L_1 \sin \beta I_2^*(L_1) + J_H^*(y_2)]. \tag{41}$$

Supposing arc BS of length y_{21} in the vertical beam is the deformed segment at the end of the first phase, we have

$$J_H^*(y_2) = J_S^*(y_{21}) + 2my_{21}L_1^2(1 - \cos \beta) + 2L_1 \sin \beta \, J_1^*(y_{21}) - 2L_1(1 - \cos \beta)J_2^*(y_{21})$$

$$+ 2mL_1^3(\beta - \sin \beta). \tag{42}$$

The energy balance leads to

$$E_{k1}^* - E_k^* = 2M_0 \beta. \tag{43}$$

According to the Notation section, the above equations can be transformed into the non-dimensional forms

$$\kappa_2 = \gamma \tag{44}$$

$$\eta_2 = \eta_{21} + \beta \, \gamma \tag{45}$$

$$V = \sqrt{\frac{\alpha E_{k1} - 2\beta}{\alpha f(\beta)}} \tag{46}$$

$$\tau = \tau_1 + \frac{1}{\alpha} \int_0^\beta \sqrt{\frac{\alpha f(\beta)}{\alpha E_{k1} - 2\beta}} \, d\beta \tag{47}$$

where

$$f(\beta) = 0.5[I_c(1) + 1 - 2I_1(1) \cos\beta + 2I_2(1) \sin\beta + \gamma^3 J_s(\eta_{21}) + 2\gamma\eta_{21}(1 - \cos\beta)$$
$$+ 2\gamma^2 \sin\beta J_1(\eta_{21}) - 2\gamma^2(1 - \cos\beta)J_2(\eta_{21}) + 2(\beta - \sin\beta)]. \tag{48}$$

The response ends when the kinetic energy is equal to zero. Hence, from (43) we have

$$\beta_f = 0.5\alpha E_{k1} \tag{49}$$

where the subscript f denotes the value of the final state.

In computing, the integration in (47) is completed by Simpson's numerical integration procedure.

After obtaining the displacement field by integrating the curvature field at any instant, the bending moment field at any instant may also be found by using the same principle. The numerical results indicate that the distribution of bending moment varies monotonously along arc CGBHA (see Fig. 2) in the first phase and along arc CBHA (see Fig. 4) in the second phase at any instant, and that the bending moment in segments CG and HA are M_0 and $-M_0$, respectively. These results imply that the solution does not violate the yield condition in the entire structure and is a complete solution.

NUMERICAL RESULTS AND COMPARISON WITH THE MODAL SOLUTION

In the following, we will compare our complete solution with the rigid–perfectly plastic approximation presented by Symonds and Raphanel (1979), which is actually a large deflection modal solution. Its deformation model corresponds to the second phase of our complete solution.

All results here are expressed in non-dimensional form. Because the length of the vertical beam does not affect the deformation model (see the Assumptions section), only the results for the case $\gamma = 1.5$ are presented.

Numerical results are summarized in Figs 5–13, where the broken lines indicate the modal solution and the full lines indicate our complete solution.

The variations of the deflection and velocity at midpoint C with time are plotted in Figs 5, 6 and 7. The deflection increases rapidly with time during the first phase, but is smaller than the modal solution because the initial velocity at point C in the modal solution is 50% larger than that in the complete solution (see Figs 6 and 7). It can be seen from Figs 6 and 7 that the time taken by the first phase is about 1/3 of the whole response time. The variation of the velocity at C with time in the complete solution at the second phase is close to that in the modal solution, and they almost coincide under the lower loading parameter $\alpha = 1.0$. This is because the curvature of the horizontal beam is small while the loading is small, and hence the results in the complete solution are closer to the modal solution.

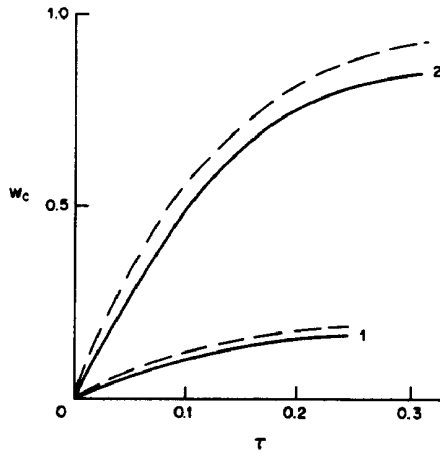Figure 8 shows the variation of the position of travelling plastic hinge G with time in

Fig. 5. Midpoint deflection vs time, $\gamma = 1.5$, (1) $\alpha = 1$, (2) $\alpha = 5$. —— Complete solution; — — — modal solution.

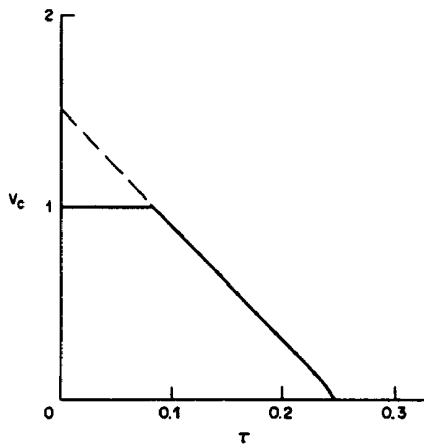

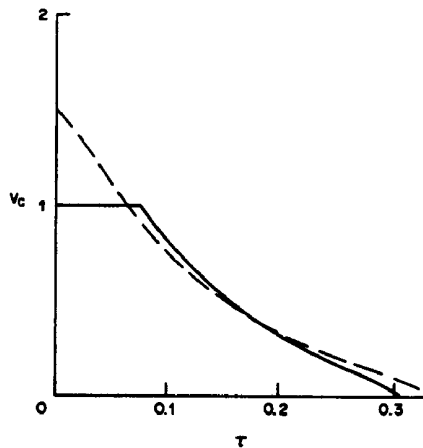Fig. 6. Midpoint velocity vs time, $\gamma = 1.5$, $\alpha = 1$. —— Complete solution; — — — modal solution.

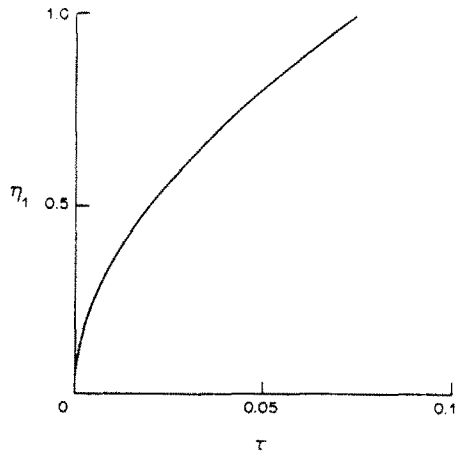Fig. 7. Midpoint velocity vs time, $\gamma = 1.5$, $\alpha = 5$. —— Complete solution; — — — modal solution.

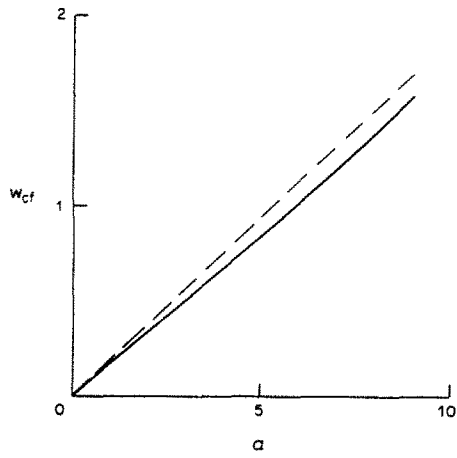Fig. 8. The position of hinge G vs time, $\gamma = 1.5$, $\alpha = 5$.

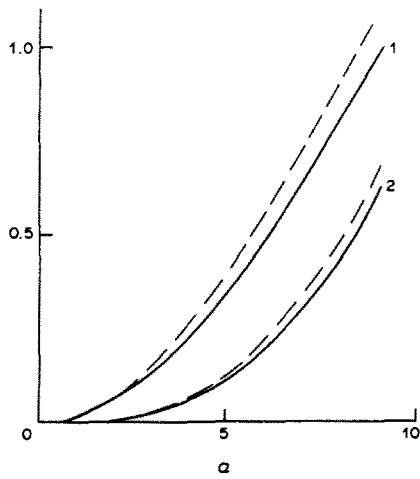Fig. 9. Final midpoint deflection vs loading parameter, $\gamma = 1.5$. —— Complete solution; – – – modal solution.

Fig. 10. Final deflection at corner B, $\gamma = 1.5$, (1) u_{Bf}, (2) w_{Bf}. —— Complete solution; – – – modal solution.

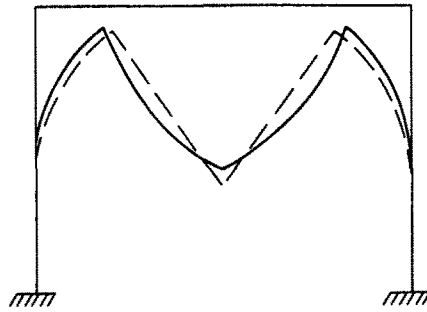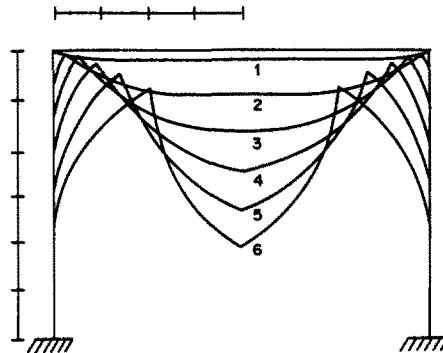Fig. 11. Final deformed shapes, $y = 1.5$, $\alpha = 5$. ⎯⎯ Complete solution; ⎯ ⎯ ⎯ modal solution.

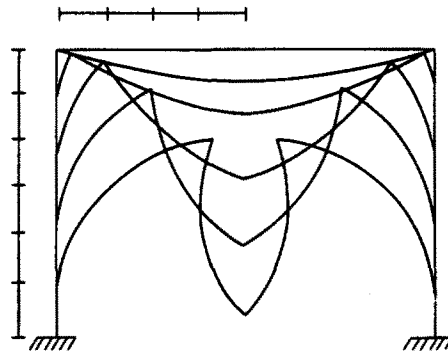Fig. 12. The evolution of the deformed shapes with time, $\gamma = 1.5$, $\alpha = 6$.

Fig. 13. Final deformed shapes under different loadings, $\gamma = 1.5$, $\alpha = 1, 2, 4, 6, 8$.

the first phase. Its travelling speed is initially equal to infinity, and then decreases gradually.

Figure 9 shows the dependence of the final deflection at midpoint C, w_{cf}, on loading parameter α. Figure 10 shows the relationship between the final displacement at corner B and loading parameter α. u_{BF} and w_{Bf} are the components of the displacement at corner B along the directions of the undeformed horizontal beam and the undeformed vertical beam, respectively.

The final deformed shapes of the frame when loading parameter $\alpha = 5$ are as plotted in Fig. 11. There is no curvature change in the horizontal beam in the modal solution because the horizontal beam does not undergo the travelling hinge phase.

From Table 1, we can see the distribution of plastic work dissipated in each portion of the structure and in each phase of the response. It indicates that most input energy is dissipated in the first phase.

In the light of Fig. 11 and Table 1, it is found that there are three dangerous regions in the portal frame: one is on the horizontal beam around the midpoint because on the

Table 1. The distribution of percentage of plastic work (%); loading parameter
$\alpha = 5$

	Midpoint	Horizontal beam	Vertical beam	Sum
First phase	0	30.8	30.8	61.6
Second phase	19.2	0	19.2	38.4
Sum	19.2	30.8	50.0	100.0

horizontal beam only the midpoint dissipates plastic work in the second phase; the other two are on two vertical beams around the corners because there is a very small bending radius at the initial stage of the response due to the initial singularity [see formula (23)]. Since the dissipated plastic work and curvature changes both concentrate in these small regions, they are the regions where failure is most likely to occur.

Figure 12 shows the evolution of the deformed shapes of the frame with time when $\alpha = 6$. Curves 1, 2 and 3 pertain to the deformed shapes in the first phase for $\eta_1 = 0.3, 0.7$ and 1.0, respectively, and curves 4, 5 and 6 pertain to the deformed shapes in the second phase for $\beta = \beta_f/3, 2\beta_f/3$ and β_f, respectively. Hence, curve 6 gives the final deformed shape of the frame.

The final deformed shapes of the frame under the different loadings are plotted in Fig. 13. From top to bottom, these curves pertain to the loading parameters $\alpha = 1, 2, 4, 6$ and 8.

The largest loading parameter for the complete solution is about $\alpha = 9$. Under this loading, corner B will finally reach the middle line of the frame (i.e. $u_{Bf} = 1$, see Fig. 10). The largest loading parameter for the modal solution is $\alpha = 8\pi/3 \doteq 8.378$.

COMPARISON WITH EXPERIMENTS

In this section, the present complete solution will be compared with the experimental results reported by Hashmi and Al-Hassani (1975) and Bodner and Symonds (1979). Their experimental data are listed in Table 2.

The effect of strain rate is neglected when the complete solution is compared with the experimental results for aluminium specimens, because aluminium is considered to be insensitive to strain rate.

Figure 14 shows the dependence of the deflection at the midpoint of the horizontal beam on the impulse of loading. The complete solution agrees well with the experimental results from aluminium specimens. The mean error between the modal solution and the experiments is slightly larger than that between the complete solution and the experiments.

The final shapes obtained from the complete solution and from the experiments using the aluminium specimens are shown in Fig. 15. The loading condition corresponds to the experimental dot marked by a letter F in Fig. 14. The discrepancy for the midpoint deflection between the complete solution and the experimental results is about 15%.

Considering that mild steel is a rate-sensitive material, as a rough approximation to this effect we may modify the complete solution by using Cowper–Symonds' law (Cowper and Symonds, 1957)

$$\dot{\varepsilon} = D(\sigma/\sigma_0 - 1)^p \tag{50}$$

where $D = 40.4$ and $p = 5.0$ are taken for mild steel according to Manjoine's experiments

Table 2. Experimental data

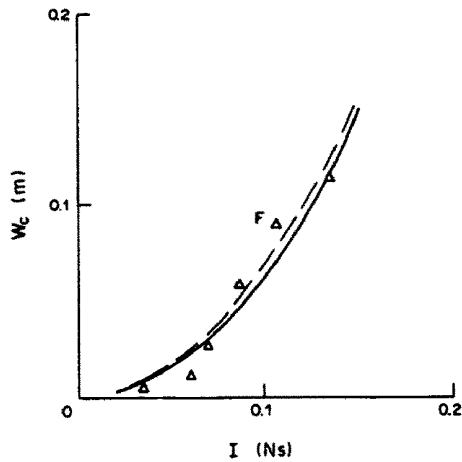| Material	L_1 (mm)	L_2 (mm)	H (mm)	b (mm)	σ_0 (MPa)	ρ (kg m^{-3})
Aluminium	66	117	0.91	12.7	83	2670
Mild steel	152	203	3.1	19.1	228	7850

Fig. 14. Final midpoint deflection vs impulse, compared with experimental results of aluminium specimens and with modal solution. —— Complete solution; — — — modal solution; △ experimental results.
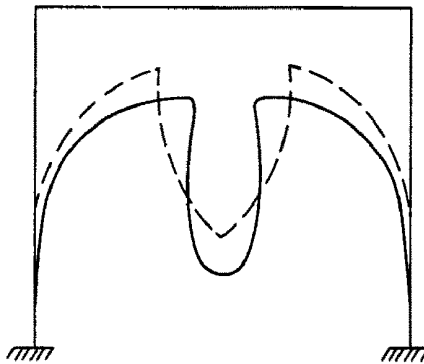

Fig. 15. Comparison of final deformed shape with experimental results of an aluminium specimen, $I = 0.1057$ Ns. —— Experiment; — — — complete solution.

(1944). In Bodner and Symonds' experiments (1979), they estimated that the experimental mean strain rate is about 5 s^{-1} in the light of measurements of the dynamic strain. Thus, the ratio $\sigma/\sigma_0 = 1.658$ is found from (50).

It is obvious from Fig. 16 that the experimental results of mild steel specimens are closer to the modified curve than to the unmodified curve.
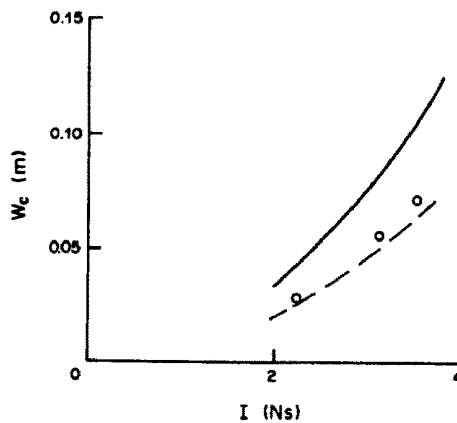

Fig. 16. Final midpoint deflection vs impulse, compared with experimental results of mild steel specimens. —— Complete solution; — — — modified complete solution by taking strain rate effect into account; ○ experiments.
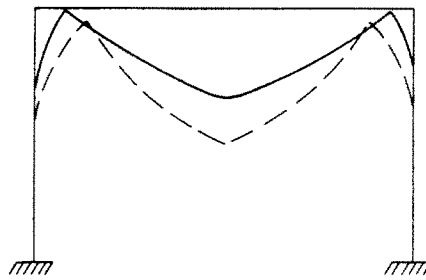
Fig. 17. Comparison of final deformed shape with experimental results of a mild steel specimen,
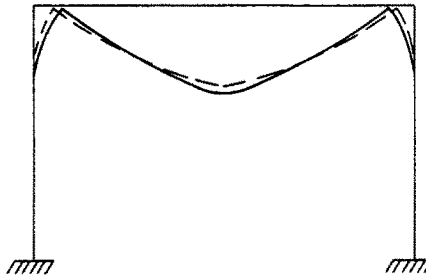$I = 3.515$ Ns. —— Experiment; – – – – complete solution.

Fig. 18. Comparison of final deformed shape with experimental results of a mild steel specimen,
$I = 3.515$ Ns. —— Experiment; – – – – modified complete solution including the strain rate effect.

The final shapes of the steel frame are plotted in Figs 17 and 18 in which, besides the experimental results, the complete solutions with and without modification due to the effect of strain rate are given. The experimental condition corresponds to the topmost experimental dot in Fig. 16.

To sum up, the rigid–perfectly plastic complete solution on the basis of a large deflection formulation is in good agreement with the experimental results.

DISCUSSIONS

(1) It is noticed from the final shape obtained from the experiments that the curvature of the portal frame under the distributed impulsive loading is generally small except in the small region near the midpoint of the horizontal beam. Hence, the assumption of small strain in the complete solution is rational for most of the frame.

(2) The assumption of large deflections in the complete solution is necessary because it is closer to the true circumstances when the frame is subjected to intense dynamic loading. As a matter of fact, if the geometrical effect of the large deflection is ignored, namely, the dynamic equations are established on the initial configuration, the axial force in the horizontal beam will be equal to zero and no force acts on the vertical beams. As a result, the vertical beams will not deform at all.

(3) The magnitude of the loading is also characterized conventionally by the energy ratio R. R denotes the ratio of the initial kinetic energy of the system to a measure of the maximum elastic strain energy that the system can store if the material is elastic–plastic, i.e.

$$R = \frac{2(0.5mL_1V_0^2)}{2(L_1+L_2)M_0^2/(2EJ)} = \frac{EJmL_1V_0^2}{M_0^2(L_1+L_2)} = \frac{EJ\alpha}{M_0(L_1+L_2)}. \tag{51}$$

After examining a one-degree-of-freedom system loaded by various pulses, Symonds pointed out that the error between adopting a rigid–plastic model and adopting an elastic–plastic model is of the order of $1/R$. Bodner and Symonds (1962) believe that the rigid–

plastic theory is a good first-order approximate theory provided $R > 3$. For large deflection dynamic plastic problems, R is generally large; for instance, R is larger than 4 in the experiments reported by Hashmi and Al-Hassani (1975) and Bodner and Symonds (1979). Hence, adopting the rigid–plastic idealization, as in this paper, should be reasonable.

(4) By analyzing the first two expressions in (21), it is found that at the initial instant the axial force of the horizontal beam, N_1, is finite, but the axial force of the vertical beam, N_2, is infinite. This is due to an initial singularity under the impulsive loading. Therefore, the influence of the axial force on yielding remains to be studied. The initial singularity caused by the initial velocity discontinuity results in not only an infinite axial force N_2 and an infinite curvature κ_2^* in the vertical beam but also a considerable shear force near the corners in the horizontal beam. However, in this paper, we ignore the effect of the shear force on the yield condition.

(5) Compared with the modal solution, the complete solution presented in this paper provides not only a better deformed shape for the frames, but also a more reasonable distribution of energy dissipation and curvature, which are important for predicting whether failure occurs or not. The modal solution can predict a reasonable final deflection at the midpoint, but its initial kinetic energy is 75% of the true initial kinetic energy and it oversimplifies the energy dissipation pattern in the frames. It may be that the final shape predicted by the complete solution still has an unrealistic cuspidal point at the midpoint of the horizontal beam, but this may be avoided if the elastic and strain-hardening behaviors are taken into account. Additional assumptions are needed to determine the strain near the midpoint.

CONCLUSIONS

(1) The rigid–perfectly plastic complete solution is constructed on the basis of a large deflection formulation for portal frames subjected to distributed impulsive loading. Possible failure regions may be found by considering the distribution of plastic work.

(2) The complete solution agrees well with the experimental results reported by Hashmi and Al-Hassani (1975) and Bodner and Symonds (1979), and the discrepancies between the complete solution and the experimental results are acceptable in engineering. This confirms that the concept of the travelling plastic hinge and the assumptions adopted in this paper are reasonable, provided the ratio R [see (51)] is large.

(3) Modified by Cowper–Symonds' law to take the strain rate effect into account, the complete solution may predict the dynamic behaviors of frames made of rate-sensitive materials well.

REFERENCES

Bodner, S. R. and Symonds, P. S. (1962). Experimental and theoretical investigation of the plastic deformation of cantilever beams subjected to impulsive loading. *J. Appl. Mech.* **29**, 719–727.

Bodner, S. R. and Symonds, P. S. (1979). Experiments on dynamic plastic loading of frames. *Int. J. Solids Structures* **15**, 1–13.

Cowper, G. R. and Symonds, P. S. (1957). Strain hardening and strain rate effects in the impact loading of cantilever beams. Technical Report No. 28 from Brown University to the Office of Naval Research under Contract No. 562(10).

Hashmi, S. J. and Al-Hassani, S. T. S. (1975). Large deflexion response of square frames to distributed impulsive loads. *Int. J. Mech. Sci.* **17**, 513–523.

Lee, E. H. and Symonds, P. S. (1952). Large plastic deformation of beams under transverse impact. *J. Appl. Mech.* **19**, 308–314.

Manjoine, M. J. (1944). Influence of rate of strain and temperature on yield stresses in mild steel. *J. Appl. Mech.* **11**, 211–218.

Symonds, P. S. and Chon, C. T. (1979). Large viscoplastic deflections of impulsively loaded plane frames. *Int. J. Solids Structures* **15**, 15–31.

Symonds, P. S. and Mentel, T. J. (1958). Impulsive loading of plastic beams with axial constraints. *J. Mech. Phys. Solids* **6**, 186–202.

Symonds, P. S. and Raphanel, J. L. (1979). Large deflections of impulsively loaded plane frame—extensions of the modal approximation technique. *Proc. conf. on mechanical properties of materials at high rates of strains*, Institute of Physics Conf., Series No. 47 (Edited by J. Harding), London and Bristol, 277–287.

Ting, T. C. T. (1965). Large deformation of a rigid, ideally plastic cantilever beam. *J. Appl. Mech.* **32**, 295–302.

Yu, T. X., Symonds, P. S. and Johnson, W. (1985). A quadrantal circular beam subjected to radial impact in its own plane at its tip by a rigid mass. *Proc. R. Soc. Lond.* **A400**, 19–36.
Yu, T. X., Symonds, P. S. and Johnson, W. (1986). A reconsideration and some new results for the circular beam impact problem. *Int. J. Impact Engng* **4**, 221–228.
Zhang, T. G. and Yu, T. X. (1986). The large rigid–plastic deformation of a circular cantilever beam subjected to impulsive loading. *Int. J. Impact Engng* **4**, 229–241.

APPENDIX

When η_1 is small in comparison with unity, θ_1 and θ_2 are small too, so that

$$\sin\theta_1 \doteq \theta_1, \quad \cos\theta_1 \doteq 1, \quad \sin\theta_2 \doteq \theta_2, \quad \cos\theta_2 \doteq 1. \tag{A1}$$

From the definitions of I_1, I_2, I_G, J_1, J_2 and J_H, it is easy to obtain an estimation of the order of these quantities, that is,

$$\begin{cases} I_1 = \eta_1^2/2, & I_2 = \kappa_1\eta_1^3/6, & I_G = \eta_1^3/3 - \kappa_1^2\eta_1^5/20 \\ J_1 = \eta_2^2/2, & J_2 = \kappa_2\eta_2^3/6, & J_H = \eta_2^3/3 - \kappa_2^2\eta_2^5/20. \end{cases} \tag{A2}$$

The first-order derivative can be taken as the first-order difference when η_1, η_2 and τ are small. Hence,

$$\dot{\eta}_1 = \eta_1/\tau \tag{A3}$$

and with the help of (15),

$$\kappa_1 = \kappa_2\frac{d\eta_2}{d\eta_1} = \kappa_2\frac{\eta_2}{\eta_1}. \tag{A4}$$

Using (23), (A4), (A2) and (30), we obtain

$$13\alpha\gamma^2(\eta_2/\eta_1)^2 + 10\alpha\gamma^3(\eta_2/\eta_1)^3 + 3\alpha\gamma^5(\eta_2/\eta_1)^5 + 120\gamma\eta_2/\eta_1^2 = 20\alpha. \tag{A5}$$

By analyzing the order of term η_2/η_1^2 in (A5), it is verified that η_2 has the same order as η_1^2 when η_1 and η_2 are small, that is,

$$\eta_2/\eta_1^2 = \alpha/6\gamma. \tag{A6}$$

Thus, it is easy to demonstrate that

$$\kappa_1 = \alpha/6. \tag{A7}$$

Using (A3), (A7) and the first equation in (29), we have

$$\eta_1 = \sqrt{6\tau}. \tag{A8}$$

Ignoring the terms with order higher than η_1^3 and using (A2) and (A8), we obtain the initial values as in (32).